Clinical Cancer Research

Co-administration of RANKL and CTLA4 Antibodies Enhances Lymphocyte-Mediated Antitumor Immunity in Mice

Elizabeth Ahern[1,2,3,4], Heidi Harjunpää[2,3], Deborah Barkauskas[1], Stacey Allen[2], Kazuyoshi Takeda[5], Hideo Yagita[6], David Wyld[3,4], William C. Dougall[1,3], Michele W.L. Teng[2,3], and Mark J. Smyth[1,3]

Abstract

Purpose: Novel partners for established immune checkpoint inhibitors in the treatment of cancer are needed to address the problems of primary and acquired resistance. The efficacy of combination RANKL and CTLA4 blockade in antitumor immunity has been suggested by recent case reports in melanoma. Here, we provide a rationale for this combination in mouse models of cancer.

Experimental Design: The efficacy and mechanism of a combination of RANKL and CTLA4 blockade was examined by tumor-infiltrating lymphocyte analysis, tumor growth, and metastasis using a variety of neutralizing antibodies and gene-targeted mice.

Results: RANKL blockade improved the efficacy of anti-CTLA4 mAbs against solid tumors and experimental metastases, with regulatory T-cell (Treg)–depleting anti-CTLA4 mAbs of the mouse IgG2a isotype showing greatest combinatorial activity. The optimal combination depended on the presence of activating Fc receptors and lymphocytes (NK cells for metastatic disease and predominantly $CD8^+$ T cells for subcutaneous tumor control), whereas anti-RANKL alone did not require FcR. The significantly higher T-cell infiltration into solid tumors post anti-RANKL and anti-CTLA4 was accompanied by increased T-cell effector function (cytokine polyfunctionality), and anti-RANKL activity occurred independently of Treg depletion. The majority of RANKL expression in tumors was on T cells whereas RANK-expressing cells were mostly tumor-associated macrophages (TAM), with some expression also observed on dendritic cells (DC) and myeloid-derived suppressor cells (MDSC).

Conclusions: These results provide a rationale for the further investigation of RANKL–RANK interactions in tumor immunity and a basis for development of translational markers of interest in human clinical trials. *Clin Cancer Res; 23(19); 5789–801. ©2017 AACR.*

Introduction

Immunotherapy has shown great promise in the treatment of certain advanced solid organ malignancies, most prominently in melanoma. Breakthrough trials using ipilimumab (a monoclonal antibody targeting CTLA4, the archetypal T-cell immune checkpoint) demonstrated, for the first time, improved survival in advanced melanoma; recent pooled analysis of long-term survival data for ipilimumab monotherapy showed a plateau of 21% in the overall survival (OS) curve commencing at about 3 years (1). More recently, adjuvant ipilimumab improved survival in stage 3 resected melanoma (2). Combining anti-CTLA4 with an mAb targeting another checkpoint, PD-1, produced superior tumor responses and survival benefit in advanced melanoma, demonstrating the importance of combination immunotherapy targeting non-redundant mechanisms of immune evasion by tumors (3–5). However, one challenge in the immunotherapy of solid cancers is the discovery of new targets for patients who display primary resistance to current immunotherapy combinations.

The possible utility of receptor activator of NF-κB ligand (RANKL) pathway blockade as a feasible therapeutic partner for anti-CTLA4 mAbs was suggested by a case report of a patient with rapidly progressive metastatic melanoma with skeletal and extra-skeletal metastasis, who received denosumab (anti-RANKL mAb) for palliation of bony pain, but then experienced an unexpected and rapid near-complete response to single agent ipilimumab (6). This report was accompanied by a preclinical experiment that showed a combination of anti-RANKL and anti-CTLA4 mAbs significantly reduced experimental mouse melanoma lung metastases via natural killer (NK) cells (6). A second case report of complete response following ipilimumab and denosumab in metastatic melanoma followed (7). However, to date the general utility and precise mechanisms of action of anti-RANKL and anti-CTLA4 have remained unclear.

[1]Immunology in Cancer and Infection, QIMR Berghofer Medical Research Institute, Herston, Queensland, Australia. [2]Cancer Immunoregulation and Immunotherapy, QIMR Berghofer Medical Research Institute, Herston, Queensland, Australia. [3]School of Medicine, University of Queensland, Herston, Queensland, Australia. [4]Medical Oncology, Royal Brisbane and Women's Hospital, Herston, Queensland, Australia. [5]Division of Cell Biology, Biomedical Research Center, Graduate School of Medicine, Juntendo University, Bunkyo-ku, Tokyo, Japan. [6]Department of Immunology, Juntendo University School of Medicine, Bunkyo-ku, Tokyo, Japan.

Note: Supplementary data for this article are available at Clinical Cancer Research Online (http://clincancerres.aacrjournals.org/).

W.C. Dougall, M.W.L. Teng, and M.J. Smyth contributed equally to this article.

Corresponding Author: Mark J. Smyth, QIMR Berghofer Medical Research Institute, 300 Herston Road, Herston, Queensland 4006, Australia. Phone: 61-7-3845-3957; Fax: 61-7-3362-0111; E-mail: Mark.Smyth@qimrberghofer.edu.au

doi: 10.1158/1078-0432.CCR-17-0606

Translational Relevance

This article illustrates the combinatorial efficacy of co-targeting RANKL and CTLA4 in mouse models of subcutaneous and metastatic cancer, predominantly in melanoma. The results provide insight into potential mechanisms of antimelanoma efficacy as described in case reports of patients receiving combination ipilimumab and denosumab in advanced melanoma, and suggest translational markers for consideration in the design of future clinical trials of similar combinations.

RANK and RANKL are members of the tumor necrosis factor receptor and ligand superfamilies, respectively, with closest homology to CD40 and CD40L. RANK (TNFRSF11a) and RANKL (TNFSF11) are currently best known in clinical practice for their role in bone homeostasis, as the differentiation of osteoclasts from the monocyte–macrophage lineage requires RANKL interaction with RANK expressed on the myeloid osteoclast precursors (8, 9). However, RANKL was initially identified as a dendritic cell (DC)–specific survival factor, which was upregulated by activated T cells and interacted with RANK on the surface of mature DCs to prevent apoptosis (10, 11). The fully human IgG2 anti-RANKL antibody (denosumab) is widely used in clinical practice as a potent and well-tolerated antiresorptive agent for the prevention of skeletal-related events arising from bone metastases, and the management of giant cell tumor of bone and osteoporosis (12, 13). Intriguingly, denosumab increased OS in a *post-hoc* exploratory analysis of a phase III trial in patients with non–small cell lung cancer and bone metastases, compared with zoledronic acid (14).

Taken together, the investigation of RANK and RANKL as possible novel immunotherapy targets in cancer is a rational approach. Here we have defined the mechanism of action of RANKL–RANK blockade in combination with anti-CTLA4, and provide insight into the combination efficacy observed in the case reports.

Materials and Methods

Cell culture

Mouse melanoma cell lines B16F10 (ATCC) and LWT1, colon cancer cell line CT26, and prostate carcinoma cell line RM-1 were maintained, injected, and monitored as previously described (15–18). The mouse prostate cancer cell line Tramp-C1 was maintained as described previously (19) but without dehydrosolandosterone. The mouse fibrosarcoma cell line MCA1956 (derived from a MCA-inoculated C57BL/6 mouse) was kindly provided by Robert Schreiber (Washington University School of Medicine, St Louis, MO). All cell lines were routinely tested negative for *Mycoplasma*, but cell line authentication was not routinely performed.

Mice

C57BL/6 wild-type (WT) mice were bred-in-house or purchased from the Walter and Eliza Hall Institute for Medical Research. C57BL/6 perforin-deficient ($pfp^{-/-}$), interferon-deficient ($IFN\gamma^{-/-}$), Fc receptor deficient (FcγRIII, FcγRIV, and FcεRγ), *Batf3* transcription factor–deficient ($Batf3^{-/-}$; ref. 20) and FoxP3-DTR (21) mice were bred in-house at the QIMR Berghofer Medical Research Institute (QIMRB). All mice were used between the ages of 6 to 16 weeks. Groups of 5 to 13 mice per experiment were used for experimental tumor metastasis assays and subcutaneous tumor growth. All experiments were approved by the QIMRB Animal Ethics Committee.

Antibodies

Purified anti-mouse anti-RANKL (IK22-5; rat IgG2a; ref. 22), anti-CTLA4 (UC10-4F10; hamster IgG) and control antibodies (1-1 or 2A3; rat IgG2a) were produced in house or purchased from BioXcell (West Lebanon, NH). Anti-CTLA4 clone 9D9 (various isotypes as indicated), and control antibody (1D12; mouse IgG2a), were supplied by Bristol–Myers Squibb. Recombinant human OPG-Fc (consisting of the ligand binding residues of OPG (residues 22–194) fused to the Fc portion of human IgG1; ref. 23) was supplied by Amgen Inc. Antibodies to deplete NK cells (anti-asialoGM1, Wako) or anti-CD8β (53.5.8, BioXcell) were administered as indicated.

Subcutaneous tumor models

For B16F10 (1×10^5), RM-1 (5×10^4), CT26 (1×10^5), MCA1956 (1×10^6) and Tramp-C1 (1×10^6) tumor formation, cells were inoculated subcutaneously into the abdominal flank of female (B16F10, MCA1956) or male (RM-1, CT26, Tramp-C1) mice. Therapeutic antibody treatment commenced as indicated on day 3 to 12 after tumor inoculation and was given every 2 to 4 days up to a maximum of 4 doses. Digital callipers were used to measure the perpendicular diameters of the tumors. The tumor size was calculated as the product of the two measurements and is presented as mean ± SEM.

Experimental lung metastasis models

Single-cell suspensions of B16F10 (2×10^5), RM-1 (1×10^5), or LWT1 (7.5×10^5) were injected intravenously into the tail vein of the indicated strains of mice. Lungs were harvested on day 14, and surface tumor nodules were counted under a dissection microscope. Antibody treatments were as indicated, with anti-CTLA4 and/or anti-RANKL mAbs administered on days −1, 0, and 2 relative to tumor inoculation. Antibodies to deplete $CD8^+$ T cells or NK cells were administered where indicated on days −1, 0, and 7 relative to tumor inoculation.

Flow cytometry

Tumor-bearing mice were sacrificed at two time points: day 9, or at end-point (when the experiment was terminated due to tumors reaching ethical endpoint size). Tumor and spleen were collected and wet weight was recorded. Single-cell suspensions were generated from indicated organs as previously described (21).

The following antibodies (from Biolegend, eBioscience, BD Biosciences) were used: CD4-BV605 (RM4-5), CD8-BV711 (53-6.7), CD11b-BV650 (M1/70), CD11b-PE (M1/70), CD11c-PE (N418), purified CD16.2 (9E9) followed by goat-anti-hamster FITC, CD206-AF647 and CD206-PECy7 (C068C2), and Zombie Aqua live/dead dye; TCRβ-PerCP-Cy5.5 (H57-597), CD45.2-A780 (104), Ly6C/Ly6G (GR-1)-EF450 (RB6-8C5), MHCII-APC (M5/114.15.2), CD265 (RANK)-PE (R12-31); RANKL-AF647 (IK22-5). For intracellular cytokine staining (ICS), cells were stimulated for 4 hours with Cell Stimulation Cocktail (1/1,000;

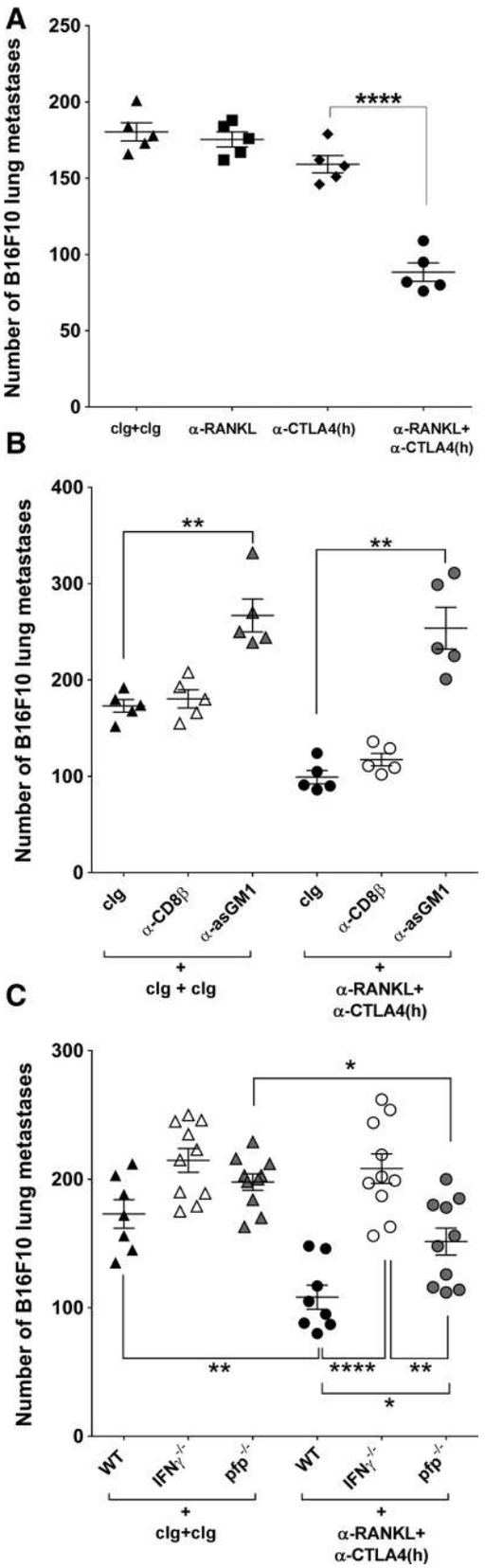

eBioscience). Cells were then surface stained as described above before being fixed/permeabilized with Cytofix/Cytoperm (BD Biosciences) and stained with IFNγ-AF488 (Biolegend), TNFα-PE (BD Biosciences), and IL-2-Pacific Blue (Biolegend).

For intracellular transcription factor staining, cells were surface stained as described above before being fixed and permeabilized using the Foxp3/Transcription Factor Staining Buffer Set (eBioscience), according to the manufacturer's protocol and stained with FoxP3-EF450 or FoxP3-AF488 (FJK-16s) and Ki67-EF450 (Sol185; eBioscience). All immune cell analysis was first gated on live, single CD45.2$^+$. T cells were defined as TCRβ$^+$NK1.1$^-$. NK cells were defined as TCRβ$^-$NK1.1$^+$. DCs were defined as CD11c$^+$MHCII^{high}cells. Tumor-associated macrophages (TAM) were defined as CD11b$^+$F4/80$^+$ non-DC cells. MDSCs were defined as CD11b$^+$, Ly6C/Ly6G (GR-1)^{hi}, non-TAM, non-DC cells. To determine absolute counts in samples, liquid-counting beads (BD Biosciences) were added immediately before samples were ran on a flow cytometer. All data were collected on a Fortessa 4 (BD Biosciences) flow cytometer and analyzed with FlowJo v10 software (Tree Star, Inc.).

Statistical analysis

GraphPad Prism and R software was used for statistical analysis. For column analyses, the Brown–Forsythe test was used to assess equal variances. If non-significant, one-way ANOVA with multiple comparisons was used. In the event of unequal variances between groups, Kruskal–Wallace analysis with Sidak's or Dunnett's multiple comparisons were employed as appropriate. For longitudinal tumor growth analysis, treatment group random effects models were used, for within-experiment mice only. Data were considered to be statistically significant where the P value was less than 0.05.

Results

Suppression of lung metastasis by CTLA4 and RANKL co-blockade depends upon NK cells and IFNγ

In mice bearing experimental B16F10 melanoma lung metastases, wild-type (WT) mice treated with the combination of hamster anti-CTLA4 (UC10-4F10) and rat anti-RANKL (IK22-5) mAbs showed superior resistance to metastases compared with mice treated with either antibody alone or control immunoglobulin (cIg; Fig. 1A). The mechanism of action of anti-CTLA4 and anti-RANKL combination therapy was determined in WT mice depleted of CD8$^+$ or NK cells or mice deficient for

Figure 1.

Suppression of experimental lung metastases by combination anti-CTLA4 and anti-RANKL is NK cell and IFNγ dependent. **A–C,** C57BL/6 wild-type (WT) or gene-targeted mice (as indicated) were injected intravenously with B16F10 melanoma cells (2×10^5), and metastatic burden was quantified in the lungs after 14 days by counting colonies on the lung surface. Mice were treated on day −1, 0, and 2 (relative to tumor inoculation) with cIg, anti-CTLA4 (UC10-4F10, hamster IgG, 200 μg i.p.) and/or anti-RANKL (IK22-5, 200 μg i.p.). Some groups of mice were additionally treated on days −1, 0, and 7 with anti-CD8β or anti-asGM1 (100 μg/mouse i.p.) to deplete CD8$^+$ T cells or NK cells where indicated. Groups of 5 to 10 mice with mean ± SEM of each group are shown. Experiments were performed once. Statistical significance as indicated was determined by one way ANOVA and Tukey's multiple comparisons (*, $P < 0.05$; **, $P < 0.01$; ****, $P < 0.0001$).

perforin or IFNγ. As shown in Fig. 1B, the efficacy of the combination relied on the presence of NK cells but not $CD8^+$ T cells; and IFNγ was critical and to a lesser extent perforin (Fig. 1C). A similar dependence on NK cells was demonstrated for the effective control of prostate carcinoma RM-1 experimental lung metastases following treatment the same with anti-CTLA4 and anti-RANKL combination therapy (Supplementary Fig. S1A).

Anti-RANKL optimally synergises with anti-CTLA4 antibodies of the IgG2a isotype

Given that the immunoglobulin constant region of anti-CTLA4 has been reported to influence antitumor activity (24), we next assessed the impact of how different anti-CTLA4 antibody isotypes synergized with anti-RANKL in suppressing experimental B16F10 lung metastases (Fig. 2). The anti-CTLA4 clone 9D9 has been produced as a number of isotypes, including mouse IgG1, IgG2a and IgG2b; whereas another isotype (IgG1-D265A) contained a mutation that eliminated binding to all Fcγ receptors (FcγR; ref. 24). As shown in Fig. 2A, the IgG2a isotype of the anti-CTLA4 (anti-CTLA4; mIgG2a) alone resulted in greater suppression of lung metastases compared with the hamster clone of anti-CTLA4 (anti-CTLA4; h), and this suppression was further increased with the addition of anti-RANKL to either anti-CTLA4 clones. Similarly, significant suppression of RM-1 and LWT1 lung metastases were also seen with anti-CTLA4 (mIgG2a) and anti-RANKL combination therapy (Supplementary Fig. S1B and S1C).

Interestingly, the other three anti-CTLA4 isotypes (IgG2b, IgG1, or IgG1-D265A) were not as effective in suppressing lung metastases as monotherapy compared with the anti-CTLA4 (mIgG2a) isotype as they did not result in significant suppression of metastases compared with the cIg treated group (Fig. 2B). However, the addition of anti-RANKL to anti-CTLA4 (h) or anti-CTLA4 (mIgG2a and mIgG2b) resulted in significant suppression of lung metastases compared with cIg. Nevertheless, the group treated with anti-RANKL and the anti-CTLA4 (mIgG2a) clone was significantly superior to the combination anti-RANKL with anti-CTLA4 (mIgG2b; Fig. 2B). Overall, anti-RANKL treatment alone did not significantly suppress metastasis, although it significantly improved the control of metastases when used in combination with specific anti-CTLA4 isotypes, most notably mIgG2a (Fig. 2A and B).

Anti-RANKL and anti-CTLA4 suppress subcutaneous tumor growth

Given these results in experimental metastasis models, the efficacy of co-administration of anti-RANKL and anti-CTLA4 mAbs in mice bearing subcutaneous tumors was next assessed (Fig. 3). Similar to the lung metastasis models, optimal B16F10 subcutaneous growth suppression by combination anti-CTLA4 and anti-RANKL was again dependent on antibody isotype, with significant suppression of growth observed with anti-CTLA4 (mIgG2a; Fig. 3A), rather than the hamster isotype (Supplementary Fig. S2A). Antitumor efficacy was also confirmed in additional subcutaneous tumor models, mouse colon cancer CT26 (Fig. 3B) and mouse prostate carcinoma Tramp-C1 (Supplementary Fig. S2B). We next performed a longitudinal analysis of seven independent pooled experiments using B16F10 comparing anti-CTLA4 (mIgG2a) or the FcγR–non-engaging clone of anti-CTLA4 (IgG1-D265A) and/or anti-RANKL with control Ig (Supplementary Fig. S2C). Overall our

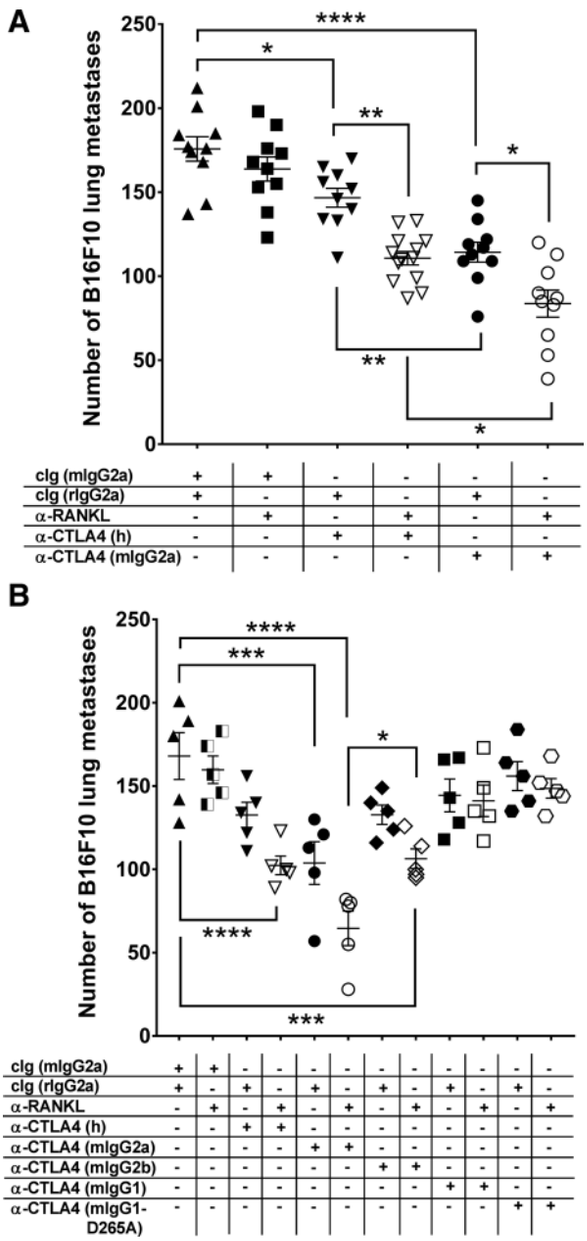

Figure 2.

Isotype of anti-CTLA4 affects combinatorial efficacy with anti-RANKL to suppress experimental lung metastases. Groups of C57BL/6 wild-type (WT) mice were injected intravenously with B16F10 melanoma cells (2×10^5) as indicated, and metastatic burden was quantified in the lungs after 14 days by counting colonies on the lung surface (**A** and **B**). Mice were treated on day −1, 0, and 2 (relative to tumor inoculation) with cIg (1D12, mouse IgG2a), various isotypes of anti-CTLA4 [UC10-4F10 (hamster IgG) or 9D9 (mouse IgG2a, IgG2b, IgG1 or IgG1 D265A), 200 μg i.p.] and/or cIg (2A3, rat IgG2a) or anti-RANKL (IK22-5, 200 μg/mouse i.p.) as indicated. Means ± SEM of 5 to 8 mice per group are shown. (**A**) is a pooled result from two independent experiments, whereas in (**B**) experiments were performed once. Statistical significance was determined by one way ANOVA, with (**A**) Tukey's multiple comparisons or (**B**) Sidak's multiple comparisons where monotherapy anti-CTLA4 is compared with cIg, and with combination with anti-RANKL, or combination with cIg (*, $P < 0.05$; **, $P < 0.01$; ***, $P < 0.001$; ****, $P < 0.0001$).

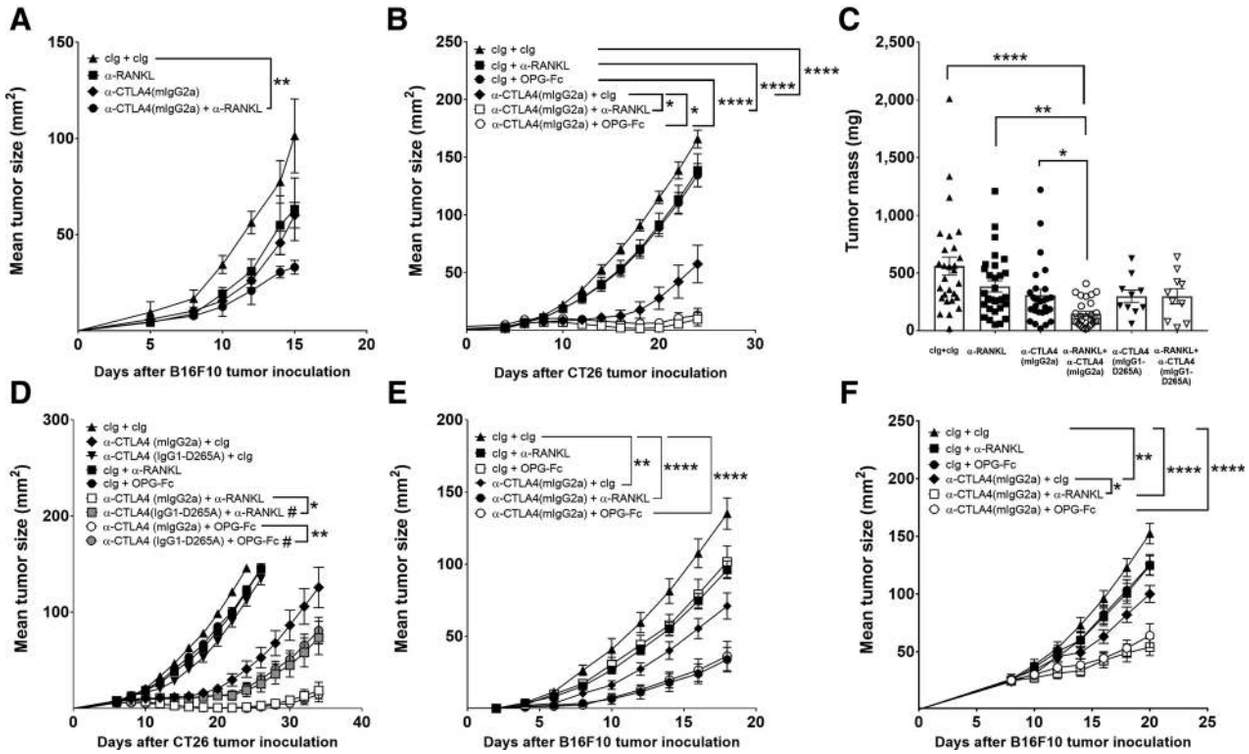

Figure 3.

The IgG2a isotype of anti-CTLA4 combines most effectively with anti-RANKL to suppress subcutaneous tumor growth. Groups of C57BL/6 wild-type (WT) mice were injected subcutaneously with (**A**, **C**, **E,** and **F**) B16F10 melanoma cells (1×10^5) or (**B** and **D**) CT26 colon cancer cells (1×10^5) and tumor growth was measured for different treatment groups. Mice were treated on (**A**, **C**, and **E**) days 3, 7, 11, and 15 (**B** and **D**) days 6, 9, 12, and 15, or (**F**) days 9, 13, 17 (relative to tumor inoculation) with cIg (1-1, rat IgG2a, 200 μg i.p.; 1D12, mouse IgG2a, 50 μg i.p.), anti-CTLA4 (9D9, mouse IgG2a or IgG1-D265A, 50 μg i.p.) and/or anti-RANKL (IK22-5, 200 μg i.p.) as indicated. Some additional groups of mice were treated i.p. with OPG-Fc (60 μg/mouse) on (**B** and **D**) days 6, 9, 12, and 15 (**E**) days 3, 6, 10, 13, and 16, or (**F**) days 9, 12, 16, and 19. B16F10 subcutaneous tumor growth (**A**, **E**, and **F**) or CT26 (**B** and **D**) subcutaneous tumor growth (displayed as means ± SEM) of 5–9 mice per group are shown. (**A**) is a representative growth curve from seven independent experiments, otherwise experiments were performed once. Statistical significance was demonstrated by one way ANOVA, Tukey's multiple comparisons, of tumor size on final day of measurement (including **D**, for combination arms only remaining at day 34; *, $P < 0.05$; **, $P < 0.01$; ****, $P < 0.0001$). In **D**, # indicates significance for the following comparisons: anti-CTLA4 (mIgG1-D265A) + anti-RANKL compared with either monotherapy, and anti-CTLA4 (mIgG1-D265A) + OPG-Fc compared with either monotherapy, at day 26. **C,** For six pooled experiments conducted as in (**A**), but not including the experiment shown in (**A**), wet tumor masses were recorded after resection from flank. Differences between combination anti-CTLA4 (mIgG2a) and anti-RANKL, either as monotherapy, or cIg were significant as indicated (Kruskal–Wallis test, Dunn's multiple comparisons, in which monotherapy arms or cIg were compared with combination anti-CTLA4 (mIgG2a) and anti-RANKL; *, $P < 0.05$; **, $P < 0.01$; ****, $P < 0.0001$).

data demonstrated the combination of anti-CTLA4 (mIgG2a) with anti-RANKL significantly suppressed tumor growth and resulted in superior efficacy compared with either as monotherapy or with cIg (Supplementary Fig. S2C). By contrast, the combination of anti-CTLA4 (IgG1-D265A) and anti-RANKL was superior to cIg-treated groups, but combinatorial therapy was not superior to either treatment as a monotherapy (Supplementary Fig. S2C). Similarly, although B16F10 tumor mass at endpoint of mice treated with combination anti-RANKL with anti-CTLA4 (mIgG2a) was also significantly decreased compared with the respective monotherapy-treated groups, there was no additive benefit of adding anti-RANKL to anti-CTLA4 (IgG1-D265A; Fig. 3C).

To confirm these findings, anti-CTLA4 mIgG2a and IgG1-D265A isotypes were assessed in the treatment of subcutaneous CT26 tumors in combination with two different therapies targeting RANKL: anti-RANKL mAb (IK22-5) or the well-validated RANKL blocker OPG-Fc (23). Anti-CTLA4 (mIgG2a) was the significantly more effective isotype in suppressing tumor growth in combination with either RANKL-directed therapy (Fig. 3D), suggesting that FcR engagement by the anti-CTLA4 mAb was required for optimal combination therapy. Similar results were found in the treatment of fibrosarcoma MCA1956 (Supplementary Fig. S2D). OPG-Fc demonstrated similar efficacy as anti-RANKL mAb when used in combination with anti-CTLA4 (mIgG2a) in CT26 (Fig. 3D) as well as B16F10 subcutaneous tumors (Fig. 3E), confirming efficacy of different RANKL-directed therapies. When treatment was commenced at a later timepoint (with established B16F10 tumors), the combinatorial efficacy of anti-CTLA4 (mIgG2a) with anti-RANKL or OPG-Fc was still observed (Fig. 3F). Despite the optimal effect of anti-CTLA-4 (mIgG2a) and anti-RANKL, in the more sensitive CT26 and MCA1956 tumor models, it was obvious that co-blockade using anti-CTLA-4 (IgG1-D265A) and anti-RANKL was also more effective than either monotherapy (Fig. 3D, Supplementary Fig. S2D). These data suggested that anti-RANKL provides additional

antitumor benefit to either Treg-depleting anti–CTLA-4 (IgG2a) or blocking only anti–CTLA-4 (IgG1-D265A) in the CT26 and MCA1956 models.

RANKL and RANK expression in the tumor microenvironment

Expression of RANKL and RANK in the B16F10 tumor microenvironment (TME) was next defined (Fig. 4A and B). The majority of intratumor RANKL was expressed by a small fraction of T cells, with a higher proportion expressing RANKL at an earlier timepoint (day 9) and higher in tumor than in spleen, with more $CD8^+$ T cells compared to $CD4^+$ T cells expressing RANKL in the tumor (Fig. 4A, Supplementary Fig. S3A). Overall, about 20% of tumor-infiltrating leukocytes (TIL) expressed RANK with greater than 90% of those also staining positive for CD11b, suggesting intratumor RANK was expressed almost exclusively by tumor-infiltrating myeloid cells (Supplementary Fig. S3B). Approximately 40% of tumor-infiltrating macrophages (TAM), 60% of MDSCs, and a low proportion of DCs (7%), expressed RANK (Fig. 4B, Supplementary Fig. S3C). Treatment with anti-RANKL did not significantly alter myeloid RANK expression on these cell types (Fig. 4B). Recently, it was reported in a B16 melanoma model that $Ly6C^{low}MHCII^{high}$ intratumor macrophages had an RNA expression profile consistent with an inflammatory M1 subtype, whereas those with $MHCII^{low/negative}$ expression were more consistent with an immunosuppressive M2 phenotype (25). Interestingly, in our B16F10 model, a higher proportion of Ly6C/Ly6G $(GR\text{-}1)^{low}$ TAMs expressing RANK had negative or low MHCII expression compared with those not expressing RANK, suggesting that the RANK-expressing TAM population may be more suppressive than those TAMs not expressing RANK (Supplementary Fig. S3D and S3E. Less than 1% of RANKL- or RANK-expressing cells are CD45.2 negative (indicating a negligible level of intratumor expression of either *in vivo*), and additionally all tumor cell lines used in this study when assessed by flow cytometry were negative for RANKL or RANK expression. Thus, RANKL and RANK expression was largely restricted to tumor-infiltrating lymphocytes and myeloid cells in the TME.

Antitumor efficacy of anti-RANKL and anti-CTLA4 (mIgG2a) combination therapy is FcγRIV receptor, IFNγ, and $CD8^+$ T-cell dependent

Next, to continue dissecting mechanism of action of the combination, we assessed the reliance of the combinatorial efficacy of anti-RANKL with anti-CTLA4 (mIgG2a) on Fc receptors and the presence and function of effector lymphocytes in the subcutaneous B16F10 tumor model (Fig. 4C). Combination activity of anti-CTLA4 (mIgG2a) and anti-RANKL against B16F10 was abrogated in mice lacking FcγRIV or FcεRγ, but not FcγRIII (Fig. 4C). This is consistent with the described mechanism of action of anti-CTLA4 (mIgG2a), which requires FcγRIV (24, 26). To determine whether Fc receptor engagement is necessary for anti-RANKL treatment alone, and because an Fc-mutant of anti-RANKL was not available, we assessed treatment effect of anti-RANKL in the immunogenic fibrosarcoma MCA1956, where anti-RANKL monotherapy resulted in significant subcutaneous growth suppression. This efficacy was preserved in mice lacking activating FcR (Supplementary Fig. S4A), demonstrating that FcR engagement was not essential for the antitumor activity of RANKL blockade. Next, the role of $CD8^+$ T cells and NK cells in the control of B16F10 tumor growth by anti-CTLA4 (mIgG2a) and anti-RANKL was assessed by the selective depletion of each subset (Fig. 4D). When $CD8^+$ T cells were depleted, the antitumor efficacy of the combination therapy was almost completely abrogated. By contrast NK-cell depletion was without effect, demonstrating the reliance of this combination therapy on $CD8^+$ T cells (Fig. 4D). Similar to results observed in the metastatic setting, this combination therapy was IFNγ dependent, but does not require perforin (Fig. 4E). The essential role for cross-presenting $CD8\alpha^+$ conventional DCs in this combination therapy was also revealed by the use of mice deficient in the transcription factor *Batf3*; the efficacy of the combination therapy was abrogated in these mice compared with WT-treated mice (Fig. 4F). Similarly, combination efficacy against subcutaneous Tramp-C1 was abrogated in $Batf3^{-/-}$ mice (Supplementary Fig. S4B).

$CD8^+$ T-cell influx into tumor post co-administration of anti-CTLA4 and anti-RANKL

To further understand the mechanism of the combination therapy and the role of $CD8^+$ T cells, the composition of TILs was assessed in subcutaneous B16F10 tumors that had been treated with the optimal combination therapy of anti-CTLA4 (IgG2a) and anti-RANKL (Fig. 5). When assessed at tumor endpoint, the proportion of $CD45.2^+$ TILs was significantly increased in the combination therapy compared with cIg- or monotherapy-treated groups (Fig. 5A). The increase in $CD45.2^+$ TILs in the combination therapy–treated group was largely accounted for by a marked increase in $CD8^+$ T cells, both in proportion (Fig. 5B) and absolute numbers (Fig. 5C).

Given the superiority of anti-CTLA4 (mIgG2a) as a partner to RANKL blockade, we next assessed the level of Tregs in the TME, as anti-CTLA4 (mIgG2a) reportedly depletes tumor-infiltrating Tregs via ADCC (24). Interestingly, although the proportion of Tregs ($CD4^+Foxp3^+$) as a percentage of $CD4^+$ T cells in the tumor was indeed reduced with anti-CTLA4 (mIgG2a) monotherapy, it was not further reduced with the addition of anti-RANKL antibody (Fig. 5D). In addition, the FcγR-IV expression on $CD11b^+$ cells was not further increased with the combination therapy in the tumor (Supplementary Fig. S5A), suggesting that enhanced Treg depletion in the TME does not explain the mechanism of action of this combination. In the spleen, no significant changes in Treg proportion or number were detected between treatment groups, indicating that Treg levels were not altered systemically with the combination (Supplementary Fig. S5B).

To further assess any essential role for Tregs in combinatorial efficacy of anti-RANKL in immunotherapy, the FoxP3-DTR mouse model was employed. In these mice, the diphtheria toxin receptor (DTR) is expressed under the control of the *foxp3* locus, allowing for the conditional and near-complete depletion of Tregs through administration of diphtheria toxin (DT), resulting in enhanced anti-tumor immunity (21). A trend to greater B16F10 subcutaneous tumor growth suppression was seen (Supplementary Fig. S5C and S5D) and a higher proportion of mice were cured when anti-RANKL therapy was given in combination with DT compared with DT alone (Supplementary Fig. S5E). In addition, a similar trend of enhanced growth suppression of subcutaneous RM-1 was also seen in FoxP3-DTR mice treated with DT and anti-RANKL (Supplementary Fig. S5F). FACS analysis of RM-1 tumors at endpoint revealed near-complete Treg depletion by DT alone, with no additional depletion of Tregs noted when anti-RANKL was

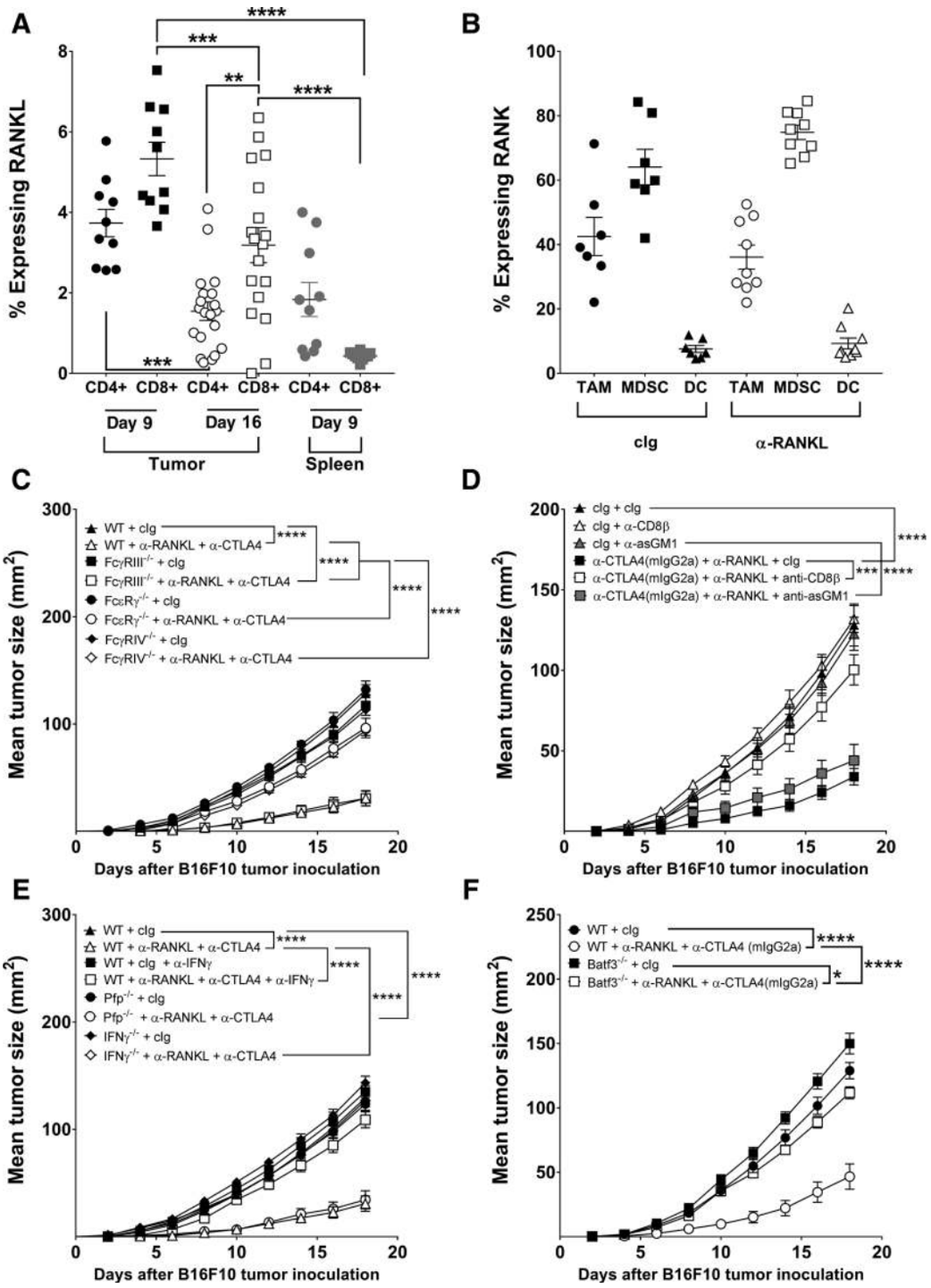

Figure 4.

Efficacy of anti-CTLA4 (mIgG2a) and anti-RANKL combination therapy is FcR-, IFNγ-, and $CD8^+$ T-cell–dependent. Groups of C57BL/6 wild-type (WT) or gene-targeted mice as indicated were injected subcutaneously with B16F10 melanoma cells (1×10^5), and tumors were harvested for FACS at (**A**) indicated time points or (**B**) day 16 after tumor inoculation, or (**C–F**) tumor growth was monitored under different treatment conditions. Mice were treated on day 3, 7, and if experiment ongoing also day 11 and 15 relative to tumor inoculation with cIg (1-1; rat IgG2a, 200 μg i.p. + 1D12; mouse IgG2a, 50 μg i.p.), anti-CTLA4 (9D9; mouse IgG2a or IgG1-D265A as indicated, 50 μg i.p.) and/or anti-RANKL (IK22-5, 200 μg i.p.) as indicated. Some mice were additionally treated intraperitoneally on days −1, 0, and 7 with anti-CD8β or anti-asGM1 (100 μg/mouse i.p.) as indicated. (**A**) Expression of RANKL by T cells, (**B**) expression of RANK by myeloid subsets indicated, and (**C–F**) B16F10 subcutaneous tumor growth (displayed as mean ± SEM) are shown for 3 to 9 mice per group. Two independent experiments, each with 3 to 10 mice per group, are combined in each of (**A–B**); otherwise experiments were performed once. Differences between groups is significant where indicated as determined by one way ANOVA, Tukey's multiple comparisons (*, $P < 0.05$; **, $P < 0.01$; ***, $P < 0.001$; ****, $P < 0.0001$). The WT groups treated with cIg and combination α-CTLA4 with α-RANKL are the same in (**C**) and (**E**) but are displayed in different graphs for ease of interpretation.

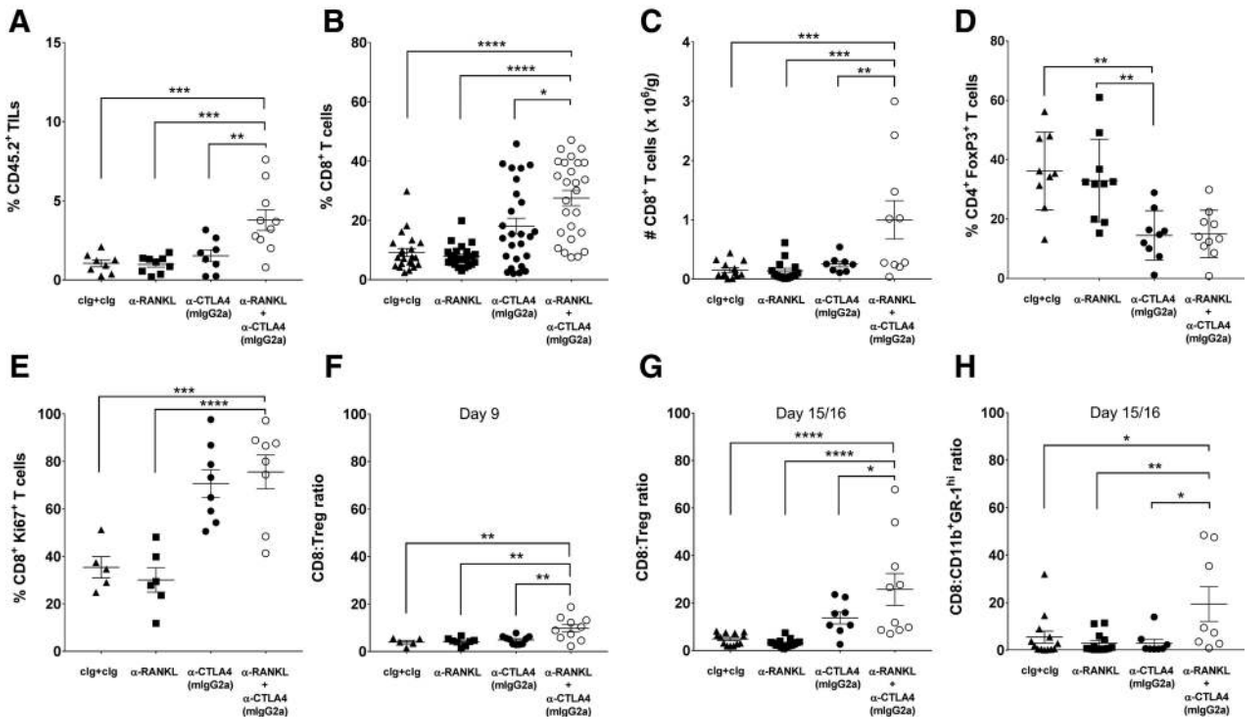

Figure 5.

Combined anti-RANKL and anti-CTLA4 therapy results in increased recruitment of $CD8^+$ T cells into tumors. Groups of C57BL/6 wild-type (WT) mice were injected subcutaneously with B16F10 melanoma cells (1×10^5) and tumors were harvested for FACS after various treatments. Mice were treated on (**A–E**, **G–H**) days 3, 7, and 11 and 15 or (**F**) days 3 and 7 relative to tumor inoculation with cIg (1-1; rat IgG2a, 200 μg i.p. + 1D12; mouse IgG2a, 50 μg i.p.), anti-CTLA4 (9D9; mouse IgG2a, 50 μg i.p.) and/or anti-RANKL (IK22-5; rat IgG2a, 200 μg i.p.) as indicated. Mice were sacrificed at (**A–E**, **G–H**) end-stage relative to ethical end-point for size (day 15 or 16) or (**F**) day 9, and tumors processed for FACS analysis. (**A**) $CD45^+$ TILs proportion of total live cells, (**B**) $CD8^+$ T cells as a proportion of total $CD45^+$ TILs, (**C**) number of intratumor $CD8^+$ T cells, (**D**) Tregs (defined as $TCR\beta^+CD4^+FoxP3^+$) as a proportion of $CD4^+$ T cells, (**E**) proportion of $CD8^+$ T cells expressing Ki-67^+, ratio of $CD8^+$ T cells to Tregs at (**F**) day 9 and (**G**) day 15 to 16, and (**H**) ratio of $CD8^+$ T cells to MDSCs for 4 to 8 mice per group are shown. Data are pooled from 2 to 5 independent experiments (**A–H**). Statistical significance where indicated was determined by (**A–C**, **E–H**) one-way ANOVA, Dunnett's multiple comparisons, or (**B**) the Kruskal–Wallis test, Dunn's multiple comparisons, where each group was compared with anti-CTLA4 (mIgG2a) + anti-RANKL combination therapy (*, $P < 0.05$; **, $P < 0.01$; ***, $P < 0.001$; ****, $P < 0.0001$).

combined with DT (Supplementary Fig. S5G). Taken together, the mechanism of action of the combination therapies in these models does not appear to be due to more efficient Treg depletion, and is intact in settings of near-complete intratumoral Treg depletion.

Another potential mechanism of action of anti-RANKL could be the enhancement of T-cell proliferation. However, we did not observe any further increase in Ki-67 expressing $CD8^+$ T cells in the combination treated groups compared to anti-CTLA4 monotherapy (Fig. 5E). This suggests that the additional $CD8^+$ T cells observed in the tumor post combination treatment might be a result of selective $CD8^+$ T cell recruitment. No significant changes were noted in proportions or numbers of myeloid subsets apart from a mild decrease in the proportion of $CD11b^+$ cells as a fraction of total TILs with combination therapy, which likely is compensatory for the increased proportion of $CD8^+$ T cells (Supplementary Fig. S6A–S6G). In addition, the proportion of TAMs expressing CD206 (an M2 marker) was not altered in either B16F10 or RM-1 subcutaneous tumors (Supplementary Fig. S6H and S6I). Influx of $CD8^+$ T cells with the combination therapy, combined with a lack of increase in suppressive immune cells such as Tregs or myeloid cells, may change the TME to favor antitumor activity. Indeed, significant increase in $CD8^+$-to-Treg ratio were noted when measured at an early time-point (day 9; Fig. 5F) or at tumor end-point (Fig. 5G). In addition, the ratio of $CD8^+$ T cells to MDSCs was also significantly increased with the combination therapy (Fig. 5H). Importantly, these observed changes were specific for the TME as no significant changes in the proportions of leukocyte subsets were observed in the spleen of these tumor-bearing mice, such as T cells (Supplementary Fig. S6J and S6K).

Anti-RANKL and anti-CTLA4 therapy increases T-cell cytokine production and polyfunctionality

Finally, given that the main changes in TME composition related to the T-cell compartment, we also assessed how this combination affected Th1 cytokine production (IFNγ, TNFα, and IL-2) from $CD8^+$ and $CD4^+$ T cells in B16F10 tumor at experimental endpoint (day 16; Fig. 6). TNFα was the most commonly produced cytokine *ex vivo* after stimulation, but significant differences were noted in the production of IFNγ by $CD8^+$ T cells (Fig. 6A) following combination therapy compared to cIg or monotherapy alone. Furthermore, $CD8^+$ T cells co-expressing IFNγ and IL-2 (Fig. 6B) or IFNγ, IL-2 and TNFα (Fig. 6C) was also increased with the combination therapy.

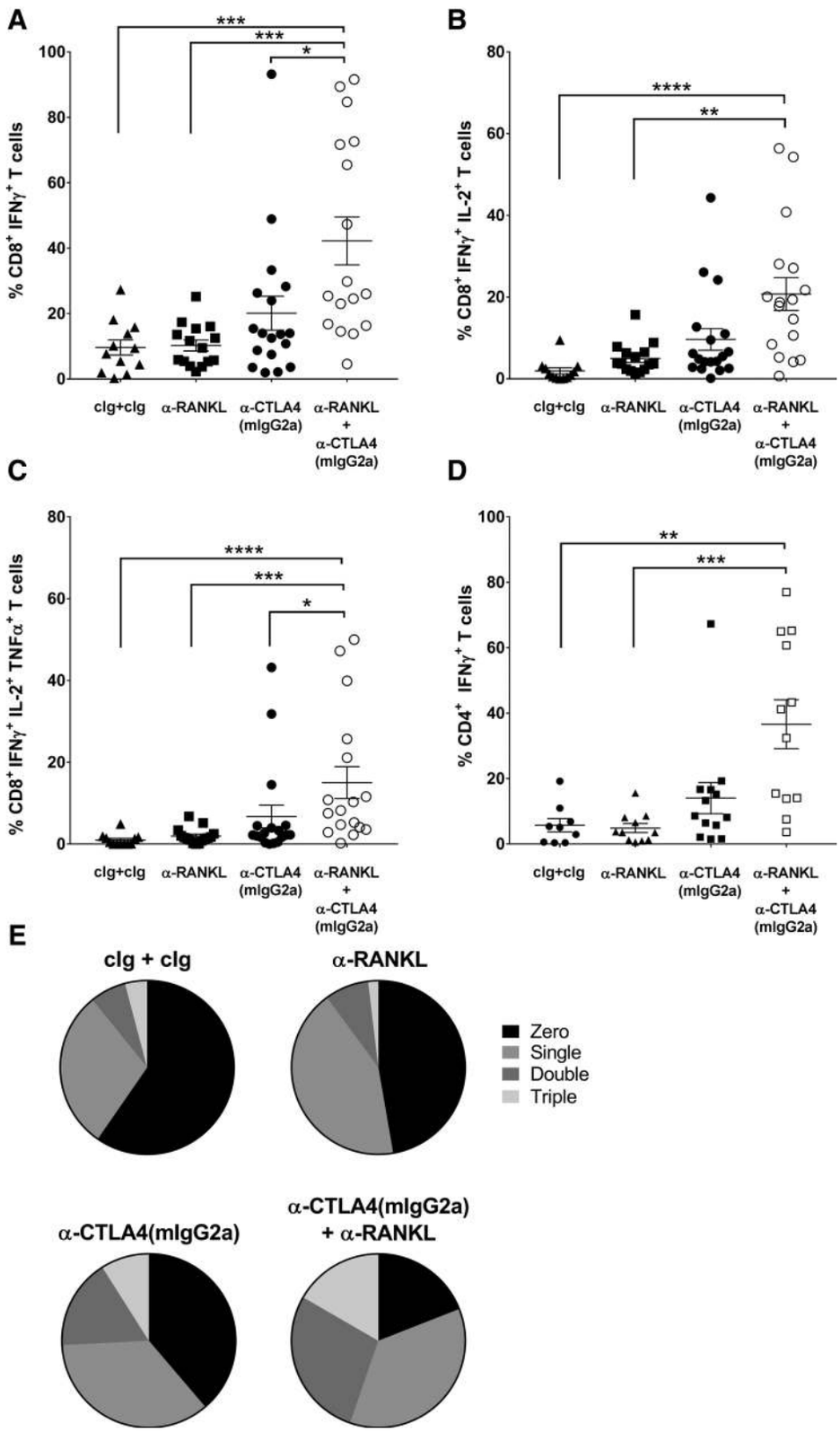

Figure 6.

Anti-RANKL improves the efficacy of anti-CTLA4 by increasing T-cell cytokine polyfunctionality. Groups of C57BL/6 wild-type (WT) mice were injected subcutaneously with B16F10 melanoma cells (1×10^5); mice were sacrificed on day 16 relative to tumor inoculation, and tumors were processed and stimulated *ex vivo* before ICS was performed for expression of cytokines. Mice were treated on days 3, 7, 11, and 15 relative to tumor inoculation with clg (1-1; rat IgG2a, 200 μg i.p. + 1D12; mouse IgG2a, 50 μg i.p.), anti-CTLA4 (9D9; mouse IgG2a, 50 μg i.p.) and/or anti-RANKL (IK22-5; rat IgG2a, 200 μg i.p.) as indicated. Proportion of $CD8^+$ T cells with positive cytoplasmic staining for (**A**) IFNγ, (**B**) IFNγ and IL-2 or (**C**) IFNγ, IL-2 and TNFα co-expression; and (**D**) proportion of $CD4^+$ T cells expressing IFNγ following the indicated therapy is shown for 4–8 mice per group. Two to three pooled independent experiments are displayed in (**A–D**). **E,** Mean proportion of $CD8^+$ T-cell–expressing zero, one, two, or three cytokines (of IFNγ, IL-2, and TNFα) from two pooled experiments is shown for each of four treatment groups as indicated. Statistical significance where indicated was determined by the Kruskal–Wallis test, Dunn's multiple comparisons where each group is compared with combination anti-CTLA4 (mIgG2a) + anti-RANKL treatment (*, $P < 0.05$; **, $P < 0.01$; ***, $P < 0.001$; ****, $P < 0.0001$).

Similar findings were also seen with $CD4^+$ T cells, particularly in the proportion that produced IFNγ (Fig. 6D). The majority of $CD8^+$ T-cell from the cIg-treated group produced no cytokines after stimulation, whereas the combination therapy generated T cells with the most polyfunctionality, with monotherapy treatment groups displaying intermediate phenotypes (Fig. 6E and Supplementary Fig. S7). The effect of the combination therapy on cytokine polyfunctionality was TME-specific, as these differences were not observed in the splenic T cells of tumor-bearing mice (Supplementary Fig. S8).

Discussion

Longer-term OS data for key immunotherapy trials in advanced melanoma are now maturing, showing encouraging results but with significant scope for improvement. Subsequent trial experience and pre-clinical studies have underlined the importance of a combinatorial approach, with superior tumor responses and survival (at 2 years) reported with combination nivolumab and ipilimumab compared with ipilimumab alone which is likely to translate into longer-term survival benefit although this data is awaited (27). A priority now is to improve combination immunotherapy to overcome primary and acquired resistance to existing therapies; experimental strategies using novel partners in combination with either ipilimumab or mAbs targeting the PD-1/PD-L1 axis have reached the clinical trial stage (28–30). In this study, we have presented data indicating the combinatorial efficacy of anti-CTLA4 with molecules blocking RANKL–RANK interactions in metastatic and subcutaneous models, and demonstrated its mechanism of action is due to increased tumor-localized $CD8^+$ T cells and enhanced effector function.

The full efficacy of CTLA4 blockade, at least in mice, relies on depletion of Tregs in addition to blocking the interaction of CTLA4 on effector T cells (Teff) with B7 ligands, which results in negative regulation of their function (31). We have shown that the optimal combinatorial efficacy of the anti-RANKL and anti-CTLA4 combination is achieved when using the anti-CTLA4 (mIgG2a) isotype. This isotype was previously demonstrated to selectively deplete intratumoral Tregs via antibody-dependent cell–mediated cytotoxicity (ADCC) involving upregulation of FcγRIV expression on $CD11b^+$ TILs, thereby enhancing antitumor immunity (24, 26). The requirement for activating FcγRs has previously been established in mice for another anti-CTLA4 isotype (9D9 mIgG2b; ref. 32), as has the requirement of FcγRIIIA in the human setting in the ex-vivo lysis of Tregs by monocytes from peripheral blood when cultured with ipilimumab (33). However, in our models, neither increased depletion of Tregs, nor further upregulation of FcγRIV on myeloid cells was seen with the combination of this IgG2a mAb with anti-RANKL. Indeed, additional efficacy of combination anti-RANKL with DT-induced Treg depletion was seen in FoxP3-DTR mice compared with DT alone, where both DT-containing arms showed >95% Treg depletion compared with cIg at endpoint. Thus, the combinatorial efficacy with anti-RANKL remained intact even when more Tregs were depleted than could be achieved through the use of anti-CTLA4 (mIgG2a), indicating that the mechanism of action of anti-RANKL was not directly on Tregs. These findings are in contrast with the previously reported roles for RANKL-expressing Tregs in the promotion of metastasis in a mouse model of RANK-expressing mammary carcinoma (34), or the role of systemic Treg control via cutaneous RANKL–RANK interactions in the restraint of UV-induced cutaneous inflammation (35). Furthermore, we have shown that monotherapy efficacy of anti-RANKL is independent of activating FcR.

Overcoming T-cell exhaustion is a hallmark of current clinically available cancer immunotherapy, with restoration of effector T-cell function (such as IFNγ production; ref. 36). In our study, blockade of RANKL when added to anti-CTLA4 further improved effector function of intratumor T cells as measured by production of Th1-type cytokines such as IFNγ and IL-2, and increased the proportion of polyfunctional T cells. Such polyfunctional T cells have been shown to be important in the control of cancer and certain chronic viral infections and vaccination (37–40). Our data demonstrated the combination therapy led to marked increase of tumor-infiltrating $CD8^+$ T cells most likely through recruitment rather than increased proliferation. In a study of human extra-mammary Paget's disease, the majority of RANK expression was associated with M2 macrophages, which produced the chemokine CCL17 when stimulated with RANKL, resulting in recruitment of T cells (41, 42). Although not addressed in this study, future analysis of chemokine production in the TME under the conditions of RANKL/RANK blockade may give further insights into this mechanism in the setting of cancer immunotherapy.

It is unclear whether the activity of anti-RANKL in combination with specific anti-CTLA4 isotypes resulted from the disruption of an immunosuppressive or tolerogenic axis between RANK-expressing myeloid cells and RANKL-expressing lymphocytes in the TME, although an essential role for DC-mediated cross-presentation was suggested through the use of *Batf3*-deficient mice. In our models, the most abundant RANK-expressing cells were TAMs, with expression also detected by DCs and MDSCs. The conditions under which myeloid cells express RANK in the TME and its downstream functions after RANK ligation remain unknown. Interactions between RANKL-expressing T cells and RANK-expressing myeloid cells can result in differential outcomes depending on factors such as anatomical site and pathologic setting. In one study, ligation of RANK on mucosal DCs by RANKL (but not splenic, mesenteric or peripheral lymph node DCs) resulted in increased IL-10 production, and oral RANKL administration at the time of antigen challenge increased oral tolerance, suggestive of a role for RANKL/RANK in tolerance induction (43). In a separate study, DCs that were co-cultured with genital squamous cell carcinoma cell lines showed an IL-10^{high} IL-12^{low} phenotype and functional deficits in a mixed lymphocyte reaction, but this phenotype could be reversed with RANKL blockade, which also resulted in increase in DC expression of co-stimulatory proteins (44). It is currently unknown whether the interaction between RANK-expressing DCs in the TME and RANKL-expressing lymphocytes results in a tolerogenic signal, although this supposition would be supported by our finding that treatment efficacy is abrogated in mice lacking *Batf3*.

RANK and RANKL are also implicated in the development of select lymphoid organs: gene-targeted mice deficient for RANK or RANKL lack peripheral lymph nodes, display thymic abnormalities, and are osteopetrotic with resultant reduction in B-cell development; in addition, a role for RANK and RANKL in the embryological development of *Aire* positive medullary thymic epithelial cells (mTEC) has been described (8, 9, 45–47). RANKL blockade as a mechanism of altering

central tolerance has been demonstrated to increase tumor antigen-specific T-cell immunity in young (3–5-week-old) mice (48). The mouse thymus reaches peak stromal cellularity at 4 weeks, and thereafter into adulthood the turnover of certain thymic epithelial cells is 10 to 14 days (49). In the current study, all mice were aged at least 6 weeks, and time from treatment commencement to experimental completion was typically 12 to 13 (but up to 20) days, meaning that alteration of thymic negative selection through depletion of mTEC subsets is unlikely to account for the antitumor efficacy of the combination studied.

The combination of RANKL blockade with alternative immune checkpoint inhibitors, such as those targeting PD-1, should now be assessed. Although the published case reports suggest unusually deep and brisk antitumor responses with combination ipilimumab and denosumab, antibodies targeting PD-1 have demonstrated superior antitumor responses compared with ipilimumab as monotherapy with a more acceptable toxicity profile (50). These results suggest that exploration of the combination of anti-RANKL and anti-PD1/PD-L1 are warranted, to assess whether the improvement of effector T-cell responses seen with the combination studied here could be recapitulated. In humans, the currently available anti-RANKL mAb is well tolerated; in cancer trials, adverse events suggestive of either immune suppression or autoimmunity were not higher than with bisphosphonate therapy (13, 51).

Overall, these results suggest a potential role for combining antibodies targeting RANKL with immune checkpoint blockade. In clinical trials of such combinations, translational markers of interest would include those of T-cell function and proliferation, and functional markers of investigational $RANK^+$ myeloid subsets. Identification of the essential RANK-expressing suppressive myeloid population(s) for combinatorial efficacy would be a key goal, as this may provide a biomarker to identify patients suitable for this approach. Furthermore, this could provide a new immunotherapeutic treatment option for patients with malignancies who currently show little response to immune checkpoint blockade, but which have a significant myeloid component in the TME, such as advanced prostate cancer (52–55).

Disclosure of Potential Conflicts of Interest

W.C. Dougall reports receiving commercial research grants from Bristol-Myers Squibb. M.W.L. Teng reports receiving speakers bureau honoraria from Merck Sharp & Dohme. M.J. Smyth reports receiving commercial research grants from Aduro Biotech, Bristol-Myers Squibb, and Corvus Pharmaceuticals, and is a consultant/advisory board member for Arcus Biosciences, F-star, and Kymab. No potential conflicts of interest were disclosed by the other authors.

Authors' Contributions

Conception and design: E. Ahern, D. Wyld, W.C. Dougall, M.W.L. Teng, M.J. Smyth

Development of methodology: E. Ahern, S. Allen

Acquisition of data (provided animals, acquired and managed patients, provided facilities, etc.): E. Ahern, H. Harjunpää, D. Barkauskas, K. Takeda, H. Yagita, M.J. Smyth

Analysis and interpretation of data (e.g., statistical analysis, biostatistics, computational analysis): E. Ahern, W.C. Dougall, M.W.L. Teng, M.J. Smyth

Writing, review, and/or revision of the manuscript: E. Ahern, D. Barkauskas, K. Takeda, H. Yagita, D. Wyld, W.C. Dougall, M.W.L. Teng, M.J. Smyth

Administrative, technical, or material support (i.e., reporting or organizing data, constructing databases): E. Ahern, S. Allen, M.W.L. Teng

Study supervision: D. Wyld, W.C. Dougall, M.W.L. Teng, M.J. Smyth

Acknowledgments

We thank Liam Town and Kate Elder for their mouse genotyping and maintenance. We also thank David Smith from the QIMR Berghofer Biostatistical Unit for statistical advice.

Grant Support

M.J. Smyth was supported by a National Health and Medical Research Council (NH&MRC) Senior Principal Research Fellowship (1078671) and The Cancer Council of Queensland (1102242). M.W.L. Teng was supported by a NHMRC Career Development Fellowship (1025552) and a QIMR-Berghofer RTCC-WEWC grant (15012). E. Ahern was supported by a University of Queensland (UQ) Australian Postgraduate Award (APA). H. Harjunpää was supported by a UQ International Postgraduate Research Scholarship, a UQ APA, and a QIMR Berghofer Top-Up award. H. Yagita was supported by a MEXT Japan grant (26290059).

The costs of publication of this article were defrayed in part by the payment of page charges. This article must therefore be hereby marked *advertisement* in accordance with 18 U.S.C. Section 1734 solely to indicate this fact.

Received March 2, 2017; revised May 23, 2017; accepted June 14, 2017; published OnlineFirst June 20, 2017.

References

1. Schadendorf D, Hodi FS, Robert C, Weber JS, Margolin K, Hamid O, et al. Pooled analysis of long-term survival data from phase II and phase III trials of ipilimumab in unresectable or metastatic melanoma. J Clin Oncol 2015;33:1889–94.
2. Eggermont AMM, Chiarion-Sileni V, Grob JJ, Dummer R, Wolchok JD, Schmidt H, et al. Prolonged survival in stage III melanoma with ipilimumab adjuvant therapy. N Engl J Med 2016;375:1845–55.
3. Larkin J, Chiarion-Sileni V, Gonzalez R, Grob JJ, Cowey CL, Lao CD, et al. Combined nivolumab and ipilimumab or monotherapy in untreated melanoma. N Engl J Med 2015;373:23–34.
4. Postow MA, Chesney J, Pavlick AC, Robert C, Grossmann K, McDermott D, et al. Nivolumab and ipilimumab versus ipilimumab in untreated melanoma. N Engl J Med 2015;372:2006–17.
5. Wolchok JD, Kluger H, Callahan MK, Postow MA, Rizvi NA, Lesokhin AM, et al. Nivolumab plus ipilimumab in advanced melanoma. N Engl J Med 2013;369:122–33.
6. Smyth MJ, Yagita H, McArthur GA. Combination anti–CTLA-4 and anti-RANKL in metastatic melanoma. J Clin Oncol 2016;34:e104–6.
7. Bostwick AD, Salama AK, Hanks BA. Rapid complete response of metastatic melanoma in a patient undergoing ipilimumab immunotherapy in the setting of active ulcerative colitis. J Immunother Cancer 2015;3:19.
8. Dougall WC, Glaccum M, Charrier K, Rohrbach K, Brasel K, De Smedt T, et al. RANK is essential for osteoclast and lymph node development. Genes Dev 1999;13:2412–24.
9. Kong YY, Yoshida H, Sarosi I, Tan HL, Timms E, Capparelli C, et al. OPGL is a key regulator of osteoclastogenesis, lymphocyte development and lymph-node organogenesis. Nature 1999;397:315–23.
10. Wong BR, Josien R, Lee SY, Sauter B, Li H-L, Steinman RM, et al. TRANCE (Tumor Necrosis Factor [TNF]-related Activation-induced Cytokine), a new TNF family member predominantly expressed in T cells, is a dendritic cell–specific survival factor. J Exp Med 1997;186:2075–80.
11. Hochweller K, Anderton SM. Kinetics of costimulatory molecule expression by T cells and dendritic cells during the induction of tolerance versus immunity *in vivo*. Eur J Immunol 2005;35:1086–96.
12. Branstetter DG, Nelson SD, Manivel JC, Blay JY, Chawla S, Thomas DM, et al. Denosumab induces tumor reduction and bone formation in patients with giant-cell tumor of bone. Clin Cancer Res 2012;18:4415–24.

13. Fizazi K, Carducci M, Smith M, Damiao R, Brown J, Karsh L, et al. Denosumab versus zoledronic acid for treatment of bone metastases in men with castration-resistant prostate cancer: a randomised, double-blind study. Lancet 2011;377:813–22.
14. Scagliotti GV, Hirsh V, Siena S, Henry DH, Woll PJ, Manegold C, et al. Overall survival improvement in patients with lung cancer and bone metastases treated with denosumab versus zoledronic acid: subgroup analysis from a randomized phase 3 study. J Thorac Oncol 2012;7: 1823–9.
15. Ferrari de Andrade L, Ngiow SF, Stannard K, Rusakiewicz S, Kalimutho M, Khanna KK, et al. Natural killer cells are essential for the ability of BRAF inhibitors to control BRAF V600E-mutant metastatic melanoma. Cancer Res 2014;74:7298–308.
16. Stagg J, Wu JH, Bouganim N, Galipeau J. Granulocyte-macrophage colony-stimulating factor and interleukin-2 fusion cDNA for cancer gene immunotherapy. Cancer Res 2004;64:8795–9.
17. Blake SJ, Stannard K, Liu J, Allen S, Yong MCR, Mittal D, et al. Suppression of metastases using a new lymphocyte checkpoint target for cancer immunotherapy. Cancer Discov 2016;6:446–59.
18. Kurtulus S, Sakuishi K, Ngiow SF, Joller N, Tan DJ, Teng MW, et al. TIGIT predominantly regulates the immune response via regulatory T cells. J Clin Invest 2015;125:4053–62.
19. Dalezis P, Geromichalos GD, Trafalis DT, Pissimissis N, Panagiotopoulou D, Galaktidou G, et al. Dexamethasone plus octreotide regimen increases anticancer effects of docetaxel on TRAMP-C1 prostate cancer model. In Vivo 2012;26:75–86.
20. Hildner K, Edelson BT, Purtha WE, Diamond M, Matsushita H, Kohyama M, et al. Batf3 deficiency reveals a critical role for CD8α(+) dendritic cells in cytotoxic T cell immunity. Science 2008;322:1097–100.
21. Teng MW, Ngiow SF, von Scheidt B, McLaughlin N, Sparwasser T, Smyth MJ. Conditional regulatory T-cell depletion releases adaptive immunity preventing carcinogenesis and suppressing established tumor growth. Cancer Res 2010;70:7800–9.
22. Kamijo S, Nakajima A, Ikeda K, Aoki K, Ohya K, Akiba H, et al. Amelioration of bone loss in collagen-induced arthritis by neutralizing anti-RANKL monoclonal antibody. Biochem Biophys Res Commun 2006;347: 124–32.
23. Lacey DL, Timms E, Tan HL, Kelley MJ, Dunstan CR, Burgess T, et al. Osteoprotegerin ligand is a cytokine that regulates osteoclast differentiation and activation. Cell 1998;93:165–76.
24. Selby MJ, Engelhardt JJ, Quigley M, Henning KA, Chen T, Srinivasan M, et al. Anti–CTLA-4 antibodies of IgG2a isotype enhance antitumor activity through reduction of intratumoral regulatory T cells. Cancer Immunol Res 2013;1:32–42.
25. De Henau O, Rausch M, Winkler D, Campesato LF, Liu C, Cymerman DH, et al. Overcoming resistance to checkpoint blockade therapy by targeting PI3Kγ in myeloid cells. Nature 2016;539:443–7.
26. Simpson TR, Li F, Montalvo-Ortiz W, Sepulveda MA, Bergerhoff K, Arce F, et al. Fc-dependent depletion of tumor-infiltrating regulatory T cells co-defines the efficacy of anti–CTLA-4 therapy against melanoma. J Exp Med 2013;210:1695–710.
27. Hodi FS, Chesney J, Pavlick AC, Robert C, Grossmann KF, McDermott DF, et al. Combined nivolumab and ipilimumab versus ipilimumab alone in patients with advanced melanoma: 2-year overall survival outcomes in a multicentre, randomised, controlled, phase 2 trial. Lancet Oncol 2016;17:1558–68.
28. Puzanov I, Milhem MM, Minor D, Hamid O, Li A, Chen L, et al. Talimogene Laherparepvec in combination with ipilimumab in previously untreated, unresectable stage IIIB-IV melanoma. J Clin Oncol 2016;34:2619–26.
29. Gangadhar TC, Hamid O, Smith DC, Bauer TM, Wasser JS, Luke JJ, et al. Preliminary results from a Phase I/II study of epacadostat (incb024360) in combination with pembrolizumab in patients with selected advanced cancers. J Immunother Cancer 2015;3(Suppl 2):O7–P453.
30. Hwu P, Hamid O, Gonzalez R, Infante JR, Patel MR, Hodi FS, et al. Preliminary safety and clinical activity of atezolizumab combined with cobimetinib and vemurafenib in BRAF V600-mutant metastatic melanoma. Ann Oncol 2016;27(suppl 6).
31. Peggs KS, Quezada SA, Chambers CA, Korman AJ, Allison JP. Blockade of CTLA-4 on both effector and regulatory T cell compartments contributes to the antitumor activity of anti–CTLA-4 antibodies. J Exp Med 2009;206: 1717–25.
32. Bulliard Y, Jolicoeur R, Windman M, Rue SM, Ettenberg S, Knee DA, et al. Activating Fc γ receptors contribute to the antitumor activities of immunoregulatory receptor-targeting antibodies. N Engl J Med 2013; 210:1685–93.
33. Romano E, Kusio-Kobialka M, Foukas PG, Baumgaertner P, Meyer C, Ballabeni P, et al. Ipilimumab-dependent cell-mediated cytotoxicity of regulatory T cells *ex vivo* by nonclassical monocytes in melanoma patients. Proc Natl Acad Sci U S A 2015;112:6140–5.
34. Tan W, Zhang W, Strasner A, Grivennikov S, Cheng JQ, Hoffman RM, et al. Tumour-infiltrating regulatory T cells stimulate mammary cancer metastasis through RANKL-RANK signalling. Nature 2011;470:548–53.
35. Loser K, Mehling A, Loeser S, Apelt J, Kuhn A, Grabbe S, et al. Epidermal RANKL controls regulatory T-cell numbers via activation of dendritic cells. Nat Med 2006;12:1372–9.
36. Quezada SA, Peggs KS, Curran MA, Allison JP. CTLA4 blockade and GM-CSF combination immunotherapy alters the intratumor balance of effector and regulatory T cells. J Clin Invest 2006;116:1935–45.
37. Almeida JR, Price DA, Papagno L, Arkoub ZA, Sauce D, Bornstein E, et al. Superior control of HIV-1 replication by $CD8^+$ T cells is reflected by their avidity, polyfunctionality, and clonal turnover. J Exp Med 2007;204: 2473–85.
38. Seder RA, Darrah PA, Roederer M. T-cell quality in memory and protection: implications for vaccine design. Nat Rev Immunol 2008;8:247–58.
39. Barber DL, Wherry EJ, Masopust D, Zhu B, Allison JP, Sharpe AH, et al. Restoring function in exhausted CD8 T cells during chronic viral infection. Nature 2006;439:682–7.
40. Blackburn SD, Shin H, Haining WN, Zou T, Workman CJ, Polley A, et al. Coregulation of $CD8^+$ T cell exhaustion by multiple inhibitory receptors during chronic viral infection. Nat Immunol 2009;10:29–37.
41. Fujimura T, Kambayashi Y, Furudate S, Asano M, Kakizaki A, Aiba S. Receptor activator of NF-kappaB ligand promotes the production of CCL17 from RANK+ M2 macrophages. J Invest Dermatol 2015;135: 2884–7.
42. Kambayashi Y, Fujimura T, Furudate S, Asano M, Kakizaki A, Aiba S. The Possible interaction between receptor activator of nuclear factor kappa-B ligand expressed by extramammary paget cells and its ligand on dermal macrophages. J Invest Dermatol 2015;135:2547–50.
43. Williamson E, Bilsborough JM, Viney JL. Regulation of mucosal dendritic cell function by receptor activator of NF-kappa B (RANK)/RANK ligand interactions: impact on tolerance induction. J Immunol 2002; 169:3606–12.
44. Demoulin SA, Somja J, Duray A, Guenin S, Roncarati P, Delvenne PO, et al. Cervical (pre)neoplastic microenvironment promotes the emergence of tolerogenic dendritic cells via RANKL secretion. Oncoimmunology 2015;4: e1008334.
45. Rossi SW, Kim MY, Leibbrandt A, Parnell SM, Jenkinson WE, Glanville SH, et al. RANK signals from CD4(+)3(-) inducer cells regulate development of Aire-expressing epithelial cells in the thymic medulla. J Exp Med 2007;204:1267–72.
46. Perlot T, Penninger JM. Development and function of murine B cells lacking RANK. J Immunol 2012;188:1201–5.
47. Kong Y-Y, Boyle WJ, Penninger JM. Osteoprotegerin ligand: a common link between osteoclastogenesis, lymph node formation and lymphocyte development. Immunol Cell Biol 1999;77:188–93.
48. Khan IS, Mouchess ML, Zhu ML, Conley B, Fasano KJ, Hou Y, et al. Enhancement of an anti-tumor immune response by transient blockade of central T cell tolerance. J Exp Med 2014;211:761–8.
49. Gray DHD, Seach N, Ueno T, Milton MK, Liston A, Lew AM, et al. Developmental kinetics, turnover, and stimulatory capacity of thymic epithelial cells. Blood 2006;108:3777–85.
50. Robert C, Schachter J, Long GV, Arance A, Grob JJ, Mortier L, et al. Pembrolizumab versus ipilimumab in advanced melanoma. N Engl J Med 2015;372:2521–32.
51. Stopeck AT, Lipton A, Body JJ, Steger GG, Tonkin K, Boer RH, et al. Denosumab compared with zoledronic acid for the treatment of bone metastases in patients with advanced breast cancer: a randomized, double-blind study. J Clin Oncol 2010;28:5132–9.
52. Kwon ED, Drake CG, Scher HI, Fizazi K, Bossi A, van den Eertwegh AJ, et al. Ipilimumab versus placebo after radiotherapy in patients with metastatic castration-resistant prostate cancer that had progressed after docetaxel chemotherapy (CA184-043): a multicentre,

randomised, double-blind, phase 3 trial. Lancet Oncol 2014;15: 700–12.
53. Topalian SL, Hodi FS, Brahmer JR, Gettinger SN, Smith DC, McDermott DF, et al. Safety, activity, and immune correlates of anti–PD-1 antibody in cancer. N Engl J Med 2012;366:2443–54.
54. Hussein MR, Al-Assiri M, Musalam AO. Phenotypic characterization of the infiltrating immune cells in normal prostate, benign nodular prostatic hyperplasia and prostatic adenocarcinoma. Exp Mol Pathol 2009;86:108–13.
55. Nonomura N, Takayama H, Nakayama M, Nakai Y, Kawashima A, Mukai M, et al. Infiltration of tumour-associated macrophages in prostate biopsy specimens is predictive of disease progression after hormonal therapy for prostate cancer. BJU Int 2011;107: 1918–22.